

Nanoscale structuring of tungsten tip yields most coherent electron point-source

Josh Y. Mutus, Lucian Livadaru, Radovan Urban, Jason Pitters, A.

Peter Legg, Mark H. Salomons, Martin Cloutier, and Robert A. Wolkow*

*Department of Physics, University of Alberta, 11322-89 Avenue, Edmonton, Alberta, T6G 2G7, Canada and
National Institute for Nanotechnology, National Research Council of Canada,
11421 Saskatchewan Drive, Edmonton, Alberta, T6G 2M9, Canada*

This report demonstrates the most spatially-coherent electron source ever reported. A coherence angle of $14.3 \pm 0.5^\circ$ was measured, indicating a virtual source size of $1.7 \pm 0.6 \text{ \AA}$ using an extraction voltage of 89.5 V. The nanotips under study were crafted using a spatially-confined, field-assisted nitrogen etch which removes material from the periphery of the tip apex resulting in a sharp, tungsten-nitride stabilized, high-aspect ratio source. The coherence properties are deduced from holographic measurements in a low-energy electron point source microscope with a carbon nanotube bundle as sample. Using the virtual source size and emission current the brightness normalized to 100 kV is found to be $7.9 \times 10^8 \text{ A/sr cm}^2$.

Electron sources have had a substantial impact on modern physics, since the invention of the cathode-ray tube well over a century ago. Now, electron sources are ubiquitous in science and industry in a variety of areas such as spectroscopy, microscopy and lithography. There have been sequential innovations in the area of nanotip fabrication and characterization [1–4].

Nanotips are of interest as field-emission electron sources as well as gas field ion sources due to their high brightness and coherence [5–7]. A high degree of coherence of such sources enables many basic applications in electron interferometry and holography, relying on splitting and self-interference of single-particle amplitudes. Essentially, these types of experiments exploit and probe first-order coherence properties, typically manifest as fringes in an interference pattern, or topological effects such as in the Ahronov-Bohm effect.

While these aspects of quantum mechanical behavior of electrons are well established, more subtle manifestations of quantum mechanics, such as those derived from second-order coherence properties of electrons and, more generally, of fermions still await detailed exploration. In this sense, the most formidable experimental challenge resides in producing sufficiently bright and coherent (therefore degenerate in the quantum mechanical sense) ensembles of fermions with well-understood interactions. A beam of freely propagating electrons qualifies as one of the best candidates for this description [8]. The beam character of this type of ensemble is particularly amenable to a great variety of experimental setups with correlated and entangled fermions from the Hanbury-Brown and Twiss experiment to the Ahronov-Bohm effect, and combinations thereof [8]. Therefore, developing more degenerate beams, such as those obtained from crafting ultrasharp metallic tips at the nanoscale, will enable among other things, a better understanding of correlated particle behavior in vacuum or in the presence of fields, a mostly uncharted experimental area. The enhanced brightness of such electron beams also open the possibility of probing ultrafast dynamics [9].

Arguably, with the availability of a highly coherent source, the most immediate application would be holographic imaging with electrons, as first recognized by Gabor [10]. Specifically, the degree of spatial coherence can be shown to be the critical limiting factor in the resolution of point-source electron holography [11, 12][33]. As it is difficult, if not impossible, to envision an electron source with a greater spatial coherence than that generated by field emission from a single atom, such emitters are now being explored extensively.

The development of techniques for creating nanotips that emit electrons from a single terminal atom have been ongoing since the first work by Fink in 1986 [1, 2]. Recently, the latter have been shown to be completely coherent: the emission across the entire opening-angle shares one phase [3]. However, although completely coherent, the emission angle for such tips remains rather small, typically a few degrees [3]. Consequently, the resulting spatial coherence of such sources has been limited by low beam divergence angles. Here we show that our single-atom tip not only has the property of being completely coherent, but also exhibits a coherence angle much larger than measured previously, and indeed than previously thought feasible [12]. This implies, among other things, a much greater resolution in the point-source holographic imaging with such a tip.

The degree of spatial coherence of an electron point source can be experimentally determined using a low-energy electron point source (LEEPS) microscope [13], a method that has been well established. The state of the art in this technique was recently described by Hwang et al.[14]

The LEEPS microscope consists of only a source, a sample and a detector. A bias is placed between a sharp metal tip and a grounded sample, causing electrons to be field emitted from the tip, past the sample and toward the detector. The coherent electron wave emitted from the tip is partially scattered off the sample, while the rest propagates towards the detector. These waves interfere at the detector to create a hologram. The width of the hologram is a measure of

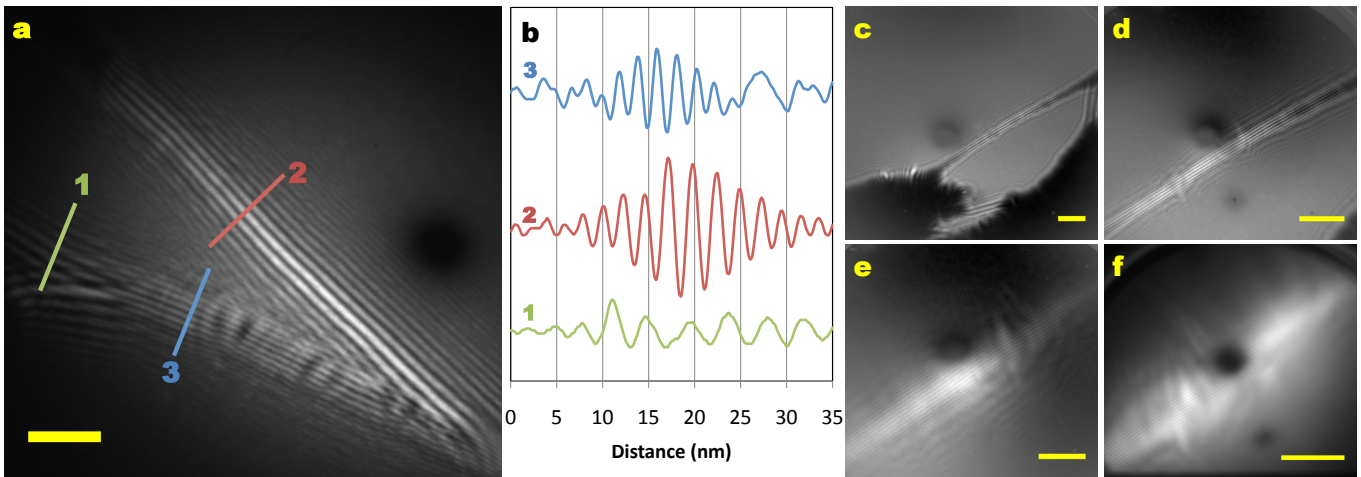


Figure 1: At low magnification the electron beam forms a broad pattern, analogous to a double slit, due to simple scattering off the bundle. This is shown in (a) (scale bar 20nm) and the corresponding line profiles in (b) where a branched bundle is imaged. (c-f) LEEPS images of carbon nanotube bundles as the tip approaches the bundle. As the magnification increases, the pattern fills the emission spot on the screen revealing complex interferometric detail. It is important to note that upon magnification fringe patterns are evident that are progressively finer from (c) to (f). Scale bars are 100 nm and 50 nm for c-d and e-f, respectively. Tip voltages and currents -122 V and 0.28 nA, -87.3 V and 0.29 nA, -89.5 V and 1.2 nA for images (d), (e) and (f) respectively.

the angular-width of the coherent wavefront emitted by the tip. As in any microscope, the numerical aperture dictates the resolution. In a LEEPS microscope, the coherence angle, α , is dictated by the character of the source. However, it is limited by many attributes of the microscope itself: uncontrolled fields and mechanical and electrical stability of the instrument can also prevent attainment of high brightness and coherence. The diffraction limited resolution, R , of the LEEPS microscope is given by:

$$R \geq \lambda/2 \sin \alpha, \quad (1)$$

where λ is the wavelength of the incident electrons. Another widely used estimate of resolution is the virtual source size, given by [13]:

$$R_v \approx \lambda/\pi\alpha. \quad (2)$$

In this paper we report on the coherence properties [34] of a nanotip made by removing material from the shank of the tip, rather than building upon it [15]. This technique uses a field-assisted, spatially-confined nitrogen etch and was reported in 2006 [16]. Such tips are not only terminated by a single tungsten atom but are uniquely stable due to the nitrogen-rich layer formed during fabrication, which coats the surface area surrounding the apex. This greatly inhibits metal diffusion and allows the tip to survive exposure to atmosphere and heating to a thousand degrees Celsius. A detailed description of the tip etching procedure can be found in the Supplementary Information

The coherence properties of the beam were measured using a custom-designed LEEPS microscope [17]. The details of its construction are the subject of a future publication. Here we give a brief description: the tip, sample and motors are contained in the scanning head. The motors are used to position the tip relative to the sample with subnanometer precision. The scanning head is suspended above a micro-channel plate (MCP). A modest, negative bias voltage (from 60-500 V, depending on the separation between tip and sample) is applied to the tip, with the sample grounded. Electrons are field-emitted from the tip, past the sample and toward the MCP some distance away. A magnified image of the region of the sample irradiated by the electrons is projected on the MCP. The image is magnified by the ratio of the tip-sample to the tip-MCP distance. In this work, the tip-MCP distance is 4 cm, but it can be varied easily from 0.5 to 20 cm by moving both tip and sample relative to the MCP.

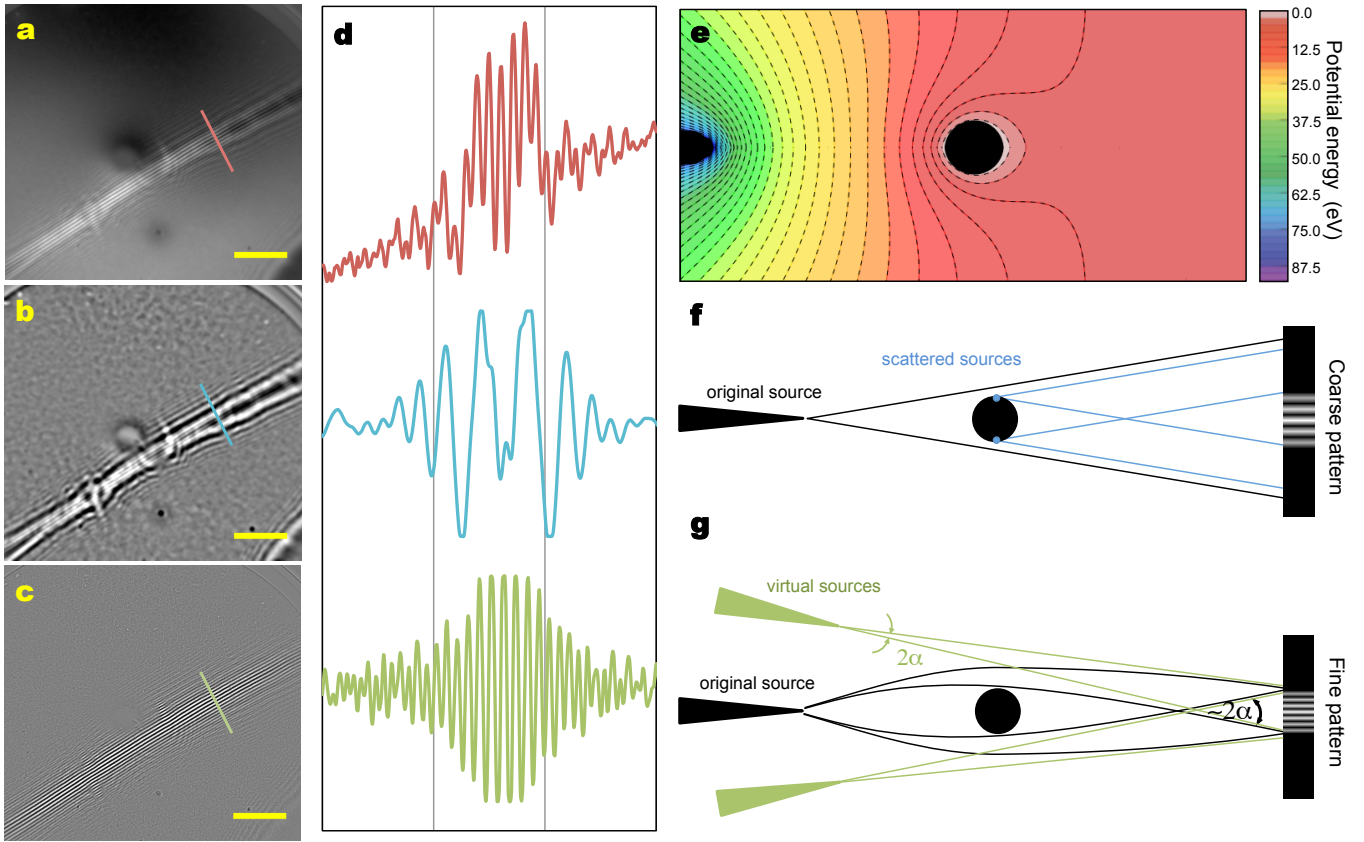


Figure 2: Filtered versions of Figure 1(d) show each fringe pattern is composed of two sets of fringes of distinct origin. Figures (b) and (c) are low-pass and high-pass filtered images of (a). Their respective line profiles are shown in (d). In order to interpret the pattern, both elastic scattering off the bundle and deflection due to the field surrounding the bundle must be considered. Equipotential surfaces between the biased tip and the grounded bundle, as shown in (e) give rise to the electron bi-prism effect. A coarse set of fringes due to scattering of the bundle itself (f) and can be explained as a simple double slit where the edges of the bundle are the sources. The fine set of fringes apparent in the image is due to the bi-prism effect shown schematically in (g). The overlap angle calculated here represents a lower bound on the coherence angle of the original beam. The pitch of the finer set of fringes can be tuned by varying the tip-sample distance and voltage as shown in the supplementary information. Scale bar is 100nm.

Carbon nanotube (CNT) bundles were suspended across holes in a 50 nm thick silicon nitride window. These windows were perforated by a regular array of $2 \mu\text{m}$ holes on a $4 \mu\text{m}$ pitch [18]. In order to make the windows conductive, they were coated in 5 nm Cr and 45 nm Au. These suspended nanotube bundles were brought into the LEEPS microscope for imaging.

The images generated by the LEEPS microscope showed two distinct fringe patterns. At low magnifications, diffraction patterns due to direct scattering off the bundle are observed. Such patterns, analogous to those from a double slit, are shown in Figure 1a and the corresponding profiles in 1b.

At higher magnifications, a finer fringe pattern becomes visible. Near the central maximum, these fringes are sinusoidally spaced and reminiscent of those generated by an electron bi-prism. In transmission electron microscopy (TEM), an electron bi-prism is made from a thin, conductive filament, biased between two grounded plates in order to create a beam-deflecting electrostatic field on each side of the filament [19]. A carbon nanotube bundle approximates this effect in LEEPS by having an electric field surrounding the bundle, due to the potential difference between the tip and bundle. This potential energy landscape is shown in Figure 2e. This experiment differs from the TEM environment where plane waves are used; in the LEEPS setup, spherical waves emanating from a point source are deflected by the bi-prism. The deflection of the beams due to the bi-prism, calculated at $5 \mu\text{Radian/V}$, is sufficient to cause the tune the overlap angle of the virtual sources and is convergent. As such, the overlap angle calculated here is represents a lower bound for the coherence angle of the original beam.

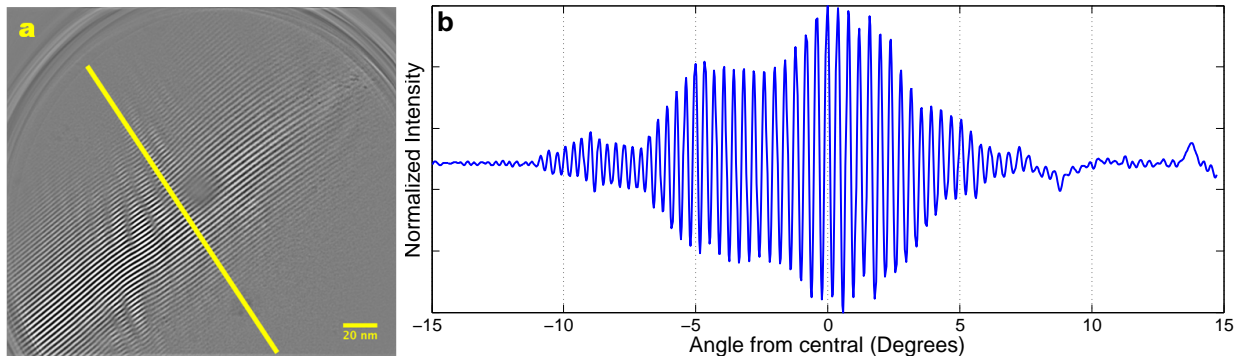


Figure 3: (a) shows a high-pass filtered version of image 1(d) (scale bar is 50nm). The interference pattern fills the detector with high-frequency fringes. High order fringes, not obvious in (a) are visible in the line profile shown in (b). The beam is completely coherent and possesses a coherence angle greater than 14° .

To describe the physics in our experimental setup, it's essential to note the interplay of three distinct types of waves (ignoring inelastically scattered and secondary waves) whose interplay gives rise to the pattern at the detector:

- (i) the unperturbed reference wave from the nanotip;
- (ii) the elastically scattered wave from the sample (this gives rise to an in-line hologram, or Fresnel diffraction, when interfering with the reference wave, and to a Young's double slit pattern, when two such waves scattered by the sample edges interfere);
- (iii) the wave deflected elastically by the electrostatic field surrounding the sample (such waves on each side of the sample giving rise to a bi-prism interference pattern). As Figure 2e shows, equipotential contours near the grounded CNT bundle are highly curved, causing electron trajectories to be turned toward the axis. The grounded supporting membrane of the sample-holder is accounted for in this calculation, but not shown in this figure, being more distant. [35]

Having laid out the principle effects at work, we can now review the presented data: at low magnification, such as Figure 1 (a), when the tip is relatively far from the CNT bundle sample, most of the electron emission from the tip passes unperturbed to the detector. A small fraction scatters off of the edges of the bundle, causing Fresnel diffraction resulting in an in-line hologram. As the magnification is progressively increased as in Figures 1 (c) through (f), two things happen which dramatically change the pattern observed at the screen:

(A) The field around the sample (scaling roughly as $U_f/\ln(d/R_0)$) increases due to smaller tip-sample separation, d , while the tip-sample bias U_f changes little (R_0 is the local radius of curvature of the CNT bundle); the angle subtended by the bi-prism field encompasses the emission area of the tip and the deflection of the beam toward the axis increases.

(B) The reference wave (i) becomes increasingly blocked by the sample itself, while the unblocked portion is increasingly deflected by the bi-prism effect, turning into wave of type (iii).

This latter effect becomes overwhelmingly dominant in cases of extreme magnification such as in Figure 1 (f), where there is no visible trace left of the shadow image or holographic fringes, indicating that all radiation reaching the detector has been deflected by the electrostatic field around the sample, and only a small fraction of radiation will forward-scatter from the edges of the sample. In this case, we have essentially a pure bi-prism experiment for a spherical electron wave emitted from a single atom. Recalling that fringe spacing is inversely related to source separation, it is observed that the relatively finely spaced fringes of 2c are consistent with the more widely spaced virtual sources of a biprism and not consistent with the double-slit scattering by the two edges of the nanotube bundle.

These results taken together illustrate that carbon nanotubes can be used to tailor the interference of the electron beam in LEEPS [20, 21] and in this work can be used to measure the coherence properties of the beam. Crucially, in the general case the fringe pattern is not purely sinusoidal because the pattern is not only due to the bi-prism; it also contains a hologram of the sample, which may or may not be distinguished in the total pattern, depending on the magnification and the potential bias applied. Optimizing and reconstructing such holograms is a future goal.

The different fringe patterns discussed above can be seen distinctly by filtering the data as shown in Figure 2 (a-c). The broader set of fringes is the Fresnel diffraction pattern from scattering off the bundle. The finer, sinusoidally-spaced fringes are due to the bi-prism effect described in equation 3 and illustrated in 2c. The two sets of fringes can be accentuated by filtering the images. The finer fringes are accentuated by using a high-pass filter, as in Figure 2c. More details of the bi-prism effect are discussed in the supplementary information.

The coherence angle (α shown in Figure 2) was measured simply by calculating

$$\tan^{-1}\left(\frac{w}{2L}\right),$$

where w was the width of the pattern on the MCP and L was the tip-MCP distance. The maximum coherence angle for these interference patterns (as shown in Figure 3) was $14.3 \pm 0.5^\circ$. This represents a marked improvement over the previous state of the art.

A high coherence angle corresponds to high transverse components of electron wavevectors and this leads to an increase in the resolution. In point-source holography this is captured in the virtual source size. Using Eq. 2 these measurements yield a virtual source size [22] of $1.7 \pm 0.6 \text{ \AA}$ [13] for emission at 89.5 V and 1.2 nA. Alternatively, the upper-bound on resolution of the LEEPS microscope can be estimated using the diffraction limit in Eq. 1. From this we expect a resolution of $2.6 \pm 0.6 \text{ \AA}$.

From the virtual source size, emission current and solid angle, all measured in the same experiment, we calculate a brightness (normalized to 100 kV) of $7.9 \times 10^9 \text{ A/sr cm}^2$. In terms of reduced brightness, this is more than four times greater than highest reported value in TEM [23]. However, this value is less than that for carbon nanotube field emitters [24], which is not surprising as the measurements reported here are based on a setup maximizing the coherence angle and not the degeneracy of the beam. We anticipate that by reducing the temperature, optimizing the extraction voltage, and further refinement of tip apex region, the degeneracy (and the reduced brightness) of our beam can be increased to a value at least two orders of magnitude greater than conventional field emission tips [8].

The reasons for the improvement in coherence angle reported here over that reported previous is not entirely known. It may be simply the result of mechanical and electrical stability of the LEEPS microscope. Great care was taken to minimize vibrations of the tip relative to the sample. The instrument has been operated in atom resolving scanning tunneling microscopy mode, demonstrating that vibrations are $\sim 0.1 \text{ \AA}$ in magnitude. This may allow the microscope to resolve higher coherence angles than previously reported. Other factors may also contribute to the attainment of higher coherence angles, such as the nature of the tip etching process. The nanotip in this work is made by removing material from the shank of the tip, rather than building a sharp protrusion upon a broad base. This results in a tip with a higher aspect-ratio. The electron emission is expected to be broader for a higher aspect-ratio tip, since an emitter with a larger radius of curvature will focus the emission into a narrow beam [7?]. Lastly, the nature of the surface of the tip itself may play a role. As the tip is etched, a protective nitrogen-rich coating remains which modifies the work function of the tip. This through a proximity effect, may play a subtle role in tuning the emission character of the tip. Further theoretical studies of these contributing factors are necessary to fully understand the novel properties of the nitrogen etched nanotip.

Whereas no previously studied point source has displayed greater than 5.5 degrees coherent opening angle [25], corresponding to approximately 1 nm [12] resolution for a LEEPS microscope, the tip described here exhibits greater than 14 degrees opening angle, indicating the potential for $\sim 1.7 \text{ \AA}$ resolution and a transformative result for electron holography by the LEEPS method. Such measurements are presently underway.

The high overall brightness of $7.9 \times 10^9 \text{ A/sr cm}^2$ at room temperature demonstrates the potential for broad applicability of this source. The coherence and the brightness properties of the nitrogen etched nanotip beam make it attractive for electron interferometry and holography both at low and high energies and as well for production of degenerate fermionic ensembles for applications requiring correlated quantum mechanical behavior. As the fabrication process is rather simple, the barrier to wider application is low.

This research was funded by the Natural Sciences and Engineering Research Council and Alberta Innovates - Technology Futures. The authors would like to thank the machine shop staff in the Physics Department at the University of Alberta for their quality work.

* Electronic address: rwalkow@ualberta.ca

[1] H. Fink, IBM journal of research and development **30**, 460 (1986).

[2] H. Fink, Physica Scripta **38**, 260 (1988).

[3] C. Chang, H. Kuo, I. Hwang, and T. Tsong, Nanotechnology **20**, 115401 (2009).

- [4] B. Cho, T. Ichimura, R. Shimizu, and C. Oshima, *Physical Review Letters* **92**, 246103 (2004), ISSN 1079-7114.
- [5] J. Pitters, R. Urban, and R. Wolkow, *The Journal of Chemical Physics* **136**, 154704 (2012).
- [6] R. Urban, J. L. Pitters, and R. A. Wolkow, *Applied Physics Letters* **100**, 263105 (2012).
- [7] R. Urban, R. A. Wolkow, and J. L. Pitters, *Ultramicroscopy* (2012).
- [8] M. Silverman, L. Ballentine, et al., *American Journal of Physics* **76**, 1078 (2008).
- [9] B. Barwick, C. Corder, J. Strohaber, N. Chandler-Smith, C. Uiterwaal, and H. Batelaan, *New Journal of Physics* **9**, 142 (2007).
- [10] D. Gabor, *Nature* **161**, 777 (1948).
- [11] G. Stevens, M. Krüger, T. Latychevskaia, P. Lindner, A. Plückthun, and H. Fink, *European Biophysics Journal* pp. 1–5 (2011).
- [12] G. Stevens, *Journal of Microscopy* **235**, 9 (2009), ISSN 1365-2818.
- [13] J. Spence, W. Qian, and M. Silverman, *Journal of Vacuum Science & Technology A: Vacuum, Surfaces, and Films* **12**, 542 (1994), ISSN 0734-2101.
- [14] I.-S. Hwang, C.-C. Chang, C.-H. Lu, S.-C. Liu, Y.-C. Chang, T.-K. Lee, H.-T. Jeng, H.-S. Kuo, C.-Y. Lin, and T. Tsong, *The New Journal of Physics* **15**, 043015 (2013).
- [15] J. L. Pitters, R. Urban, C. Vesa, and R. A. Wolkow, *Ultramicroscopy* (2013).
- [16] M. Rezeq, J. Pitters, and R. Wolkow, *The Journal of chemical physics* **124**, 204716 (2006).
- [17] J. Mutus, L. Livadaru, J. Robinson, R. Urban, M. Salomons, M. Cloutier, and R. Wolkow, *New Journal of Physics* **13**, 063011 (2011).
- [18] S. P. Inc, p/N 4108PSN-BA.
- [19] H. Lichte and M. Lehmann, *Reports on Progress in Physics* **71**, 016102 (2008).
- [20] V. Georges, J. Bardon, A. Degiovanni, and R. Morin, *Ultramicroscopy* **90**, 33 (2001).
- [21] M. Prigent and P. Morin, *Journal of microscopy* **199**, 197 (2000), ISSN 1365-2818.
- [22] M. Scheinfein, W. Qian, and J. Spence, *Journal of applied physics* **73**, 2057 (1993).
- [23] T. Kawasaki, T. Yoshida, T. Matsuda, N. Osakabe, A. Tonomura, I. Matsui, and K. Kitazawa, *Applied Physics Letters* **76**, 1342 (2000).
- [24] N. De Jonge, *Journal of applied physics* **95**, 673 (2004).
- [25] J. Longchamp, T. Latychevskaia, C. Escher, and H. Fink, *Applied Physics Letters* **101**, 113117 (2012).
- [26] A. Götzhäuser, B. Völkel, B. Jäger, M. Zharnikov, H. Kreuzer, and M. Grunze, *Journal of Vacuum Science & Technology A: Vacuum, Surfaces, and Films* **16**, 3025 (1998).
- [27] P. Morin, M. Pitaval, and E. Vicario, *Physical Review Letters* **76**, 3979 (1996).
- [28] M. Prigent and P. Morin, *Journal of Physics D: Applied Physics* **34**, 1167 (2001).
- [29] C. Oshima, E. Rokuta, and B. Cho, *Chinese Journal of Physics* **43** (2005).
- [30] F. Hasselbach, *Reports on Progress in Physics* **73**, 016101 (2010).
- [31] H. Lichte, *Journal of electron microscopy* **47**, 387 (1998).
- [32] R. Fowler and L. Nordheim, *Proceedings of the Royal Society of London. Series A, Containing Papers of a Mathematical and Physical Character* **119**, 173 (1928).
- [33] Degeneracy, coherence and brightness of a point source are all inextricably related as they all depends on the virtual source size. Thus, minimizing the latter is key to maximizing the related quantities.
- [34] While many published results in this area have put measurements in terms of half-width-at-half-maximum, in this work we quote the coherence angle as the half-width of the entire pattern. This enables us to put our measurements easily in context of the Numerical Aperture (NA) of the microscope since each fringe present in the image present in the pattern will contribute to the overall resolution of the reconstructed hologram. A comparison of our work to landmark works in the literature can be found in Table I contained in the Supplementary Information.
- [35] Electrostatic calculations were performed for the shown geometry using the finite element method. Dirichlet boundary conditions were used for the tip, CNT and supporting membrane. A custom mesh was employed to accurately capture the regions of high field.

Supplementary information

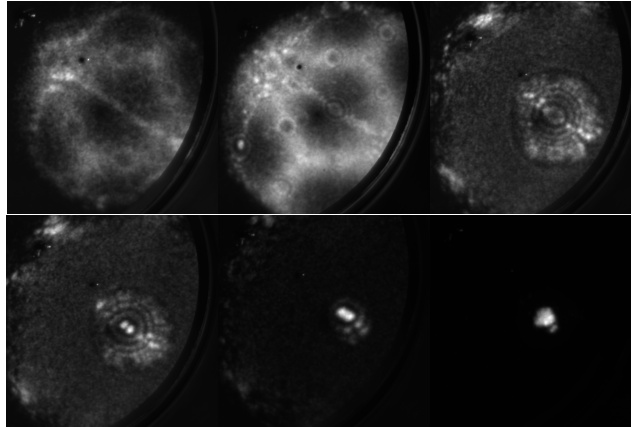
I. COMPARISON WITH OTHER SOURCES

Reference	Emission HWHM	Pattern HWHM	Geometry limited maximum angle	Coherence angle
[26]	-	1.6°	~8°	~3°
[24]	-	-	1.6°	1.4°
[21, 27, 28]	-	-	1.4°	-
[29]	3.3°	3.3°	4.3°	too large for detector
[3, 14]	2.3°	2.3°	12.8°	-
[25]	-	-	NA=0.48, 30°	5.5°
This work	7.25°	7.25°	variable	14.5°

Table I: A comparison of coherence angle from other works

There are many previous measurements of coherence angle, a broad selection are shown in Table I. Some of these quantities are quoted directly from the referenced papers, where in other cases they had to be calculated from information provided about the experimental apparatus. This is compiled in order to compare our work using the same figures of merit presented in the literature.

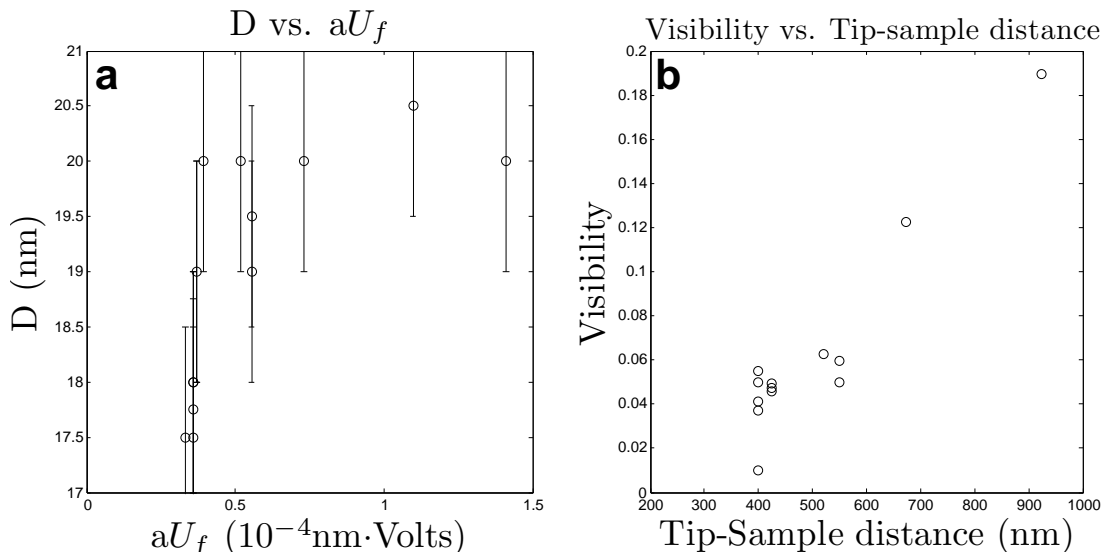
II. TIP ETCHING



Supplementary Figure 1: FIM images showing the etching of the tip. Imaging voltages are 13.0 kV, 6.50 kV, 6.10 kV, 5.35kV, 5.05kV for each image, respectively

To create such the tip used in the experiment, nitrogen gas is leaked into the system under field-ion microscope (FIM) observation. Nitrogen reacts with the tungsten, causing small protrusions. The field at these protrusions is high enough to cause field-desorption - removing the material. The high-fields used during the etching process inhibit nitrogen from migrating near the apex. As a result the reaction and field-desorption to occur preferentially at the shank of the tip. What remains is a sharp apex with a higher aspect-ratio than single-atoms tips fabricated using previous methods [7?][5].

The tips in this work were etched using a specific recipe. Before applying the field-assisted nitrogen technique, a relatively sharp tip with a radius of curvature $>10\text{nm}$ was first obtained by electrochemically etching a polycrystalline tungsten wire in NaOH. The tip was then loaded into an ultra-high vacuum (UHV) chamber with a base pressure of 1×10^{-10} Torr and placed in a LN₂ cooled FIM setup. A high voltage was applied on the tip and a background pressure of 1×10^{-5} Torr of helium was leaked into the chamber. A bias voltage between 10-20 kV was necessary to obtain a clean, stable FIM image of the tip. A background pressure of 2×10^{-6} Torr of nitrogen was then introduced into the



Supplementary Figure 2: The fine fringe pattern is generated by electrons that do not scatter off the nanotube bundle but instead are deflected by the electric field surrounding it. This results in a bi-prism mode, analogous to that of the double slit, where the effective slit separation can be tuned by changing the bias between the tip and the bundle. This is illustrated in 2(g). As the field increases, so does the separation of the virtual sources, resulting in a finer fringe pattern. (a): demonstrates the dependence of the effective source separation on tip-bundle bias U_f and separation a . (b) The visibility of the fringe patterns falls off linearly with tip-sample distance. This fits the conjecture that the reduced visibility is simply due to obstruction of the coherence electron wave by the nanotube bundle.

chamber. The bias voltage was held constant for 45 minutes. This allowed the material along the shank of the tip outside of the FIM image, to be etched away. The voltage was then decreased automatically at a rate of 1 V/s, until the bias reached 5.5 kV. When it was evident from the FIM image that etching had reached a standstill, the voltage was lowered in 100 V increments at 1 V/s. When the voltage reached 5 kV, the N_2 pressure was lowered to 8×10^{-7} Torr and the voltage was lowered in 10 V increments until the tip was sufficiently sharp, typically ending in a single atom.

III. INTERPRETATION OF FRINGE PATTERNS

The electron trajectories are bent towards the optical axis by the electric field resulting in an interference pattern analogous to that of the double slit, where the slit separation is tuned by varying the voltage between tip and bundle [30, 31]. This is shown schematically in Figure 2g. The angular intensity of the interference pattern can be expressed as:

$$I(\alpha) = 4I_o \cos^2 \left(\frac{4\pi a \gamma_o U_f}{\lambda} \alpha \right), \quad (3)$$

where a is the tip-bundle distance, U_f is the relative bias between tip and sample, λ is the deBroglie wavelength of the electron and γ_o is the angular deflection per Volt characteristic of the bi-prism. The bi-prism can be expressed as a double slit with an effective slit separation of $D = a\gamma_o U_f$. The pitch of the fringe pattern can be changed by tuning the voltage of the tip relative to the bundle, as is shown in Supplementary Figure 2. Practically, the tip-sample distance, extraction voltage and current are related by the Fowler-Nordheim equation [32]. The tip can only be operated safely in a narrow window for beam current ranging between 0.03 - 2 nA. This limits the amount we can explore the dependence of the pattern on these variables. These finer fringe patterns are only revealed at higher magnifications and are evident in Figures 1, 2, and 3.

It also must be noted that the visibility of the fringe patterns falls off linearly as magnification increases as seen in Supplementary Figure 2b. While increased visibility has been previously seen with reduced temperature of the emitter [4], we doubt that the drop off in visibility is due to a change in the coherence properties of the source itself.

This can be more simply explained by considering the geometry of the experiment. As the magnification increases, the tip is brought closer to the nanotube bundle, resulting in an increased fraction of the beam being blocked by the tube. This results in a greater fraction of electrons being absorbed or incoherently scattered by the metallic nanotube bundle. This yields a smaller fraction of coherent electron irradiation to contribute to the pattern, hence the reduced visibility. This conjecture fits with the linear fall off of visibility demonstrated in Supplementary Figure 2b: the solid angle (and therefore the number of electrons) eclipsed by the bundle would vary linearly with tip-sample distance. This lack of visibility due to the gross size of the sample also limits the application of holographic reconstruction to this sample.